Design and Optimization of a Graphene Filter for Resonant Modes in a Silicon Nitride Waveguide (GRAMO)

Andrés Manuel Sánchez-Toril

7 June 2024

Abstract

In this work, it is reported the design and optimization of graphene-on-silicon nitride integrated waveguide mode filters for suppressing the propagation of either TE_0 or TE_1 modes. The integrated waveguide consists of a silicon nitride waveguide partially covered by single layer graphene films. The physical details of graphene and its implementation in simulation software for studying the properties of this material in optical waveguides and their use for mode filtering will be addressed. This project presents the work plan followed, along with an explanation of the software usage, the results obtained, and their discussion. Finally, conclusions are drawn on the feasibility and usefulness of these types of filters, current research advancements, and their potential applications.

Índice

Índice de figuras

Índice de ecuaciones

1. Introduction

Photonic devices integrating graphene in waveguides have shown great potential for optical communication applications since 2010 [3], due to the unique optical and electrical properties of the material [4]. This integration can help overcome some limitations of conventional silicon-based photonic integrated circuits (PIC), demonstrating significant potential for applications such as high-speed and broadband photodetectors and electro-optical modulators [5–7].

Particularly noteworthy is mode-division multiplexing (MDM) technology, as it opens up the possibility of increasing the transmission capacity of communications through a waveguide by modulating multiple channels into different modes of the propagating electromagnetic field [8]. Compared to wavelength-division multiplexing technology, MDM technology does not require multiple laser sources at precise wavelengths and provides a cost-effective method to scale capacity.

To study a possible implementation of this technology, some researchers have considered fabricating silicon nitride (SiN) waveguides due to their compatibility with CMOS manufacturing and their ultra-low losses and relatively large fabrication tolerance compared to silicon [2, 9].

The general objective of this work is to use graphene sheets for the design and study of filters for TE_0 and TE_1 modes in a rectangular optical waveguide operating at a wavelength of $\lambda = 1550$ nm.

For this purpose, the commercial simulation software COMSOL Multiphysics will be used, a simulator that, using the finite element method (FEM), will enable the characterization of the optical waveguide. This study will first be conducted for a case without graphene to optimize the dimensions for the propagation of only the modes of interest and obtain the electric field values in the waveguide core. Subsequently, the values found will be used as a reference to study the efficiency of graphene as an absorber depending on the sheet width, and the surface conductivity method will be used to analyze how changes in key graphene parameters affect mode absorption.

2. Methodology and Development

2.1. Work Organization

To achieve the objectives, an organizational chart outlining the tasks was first created, as shown in Figure 1.

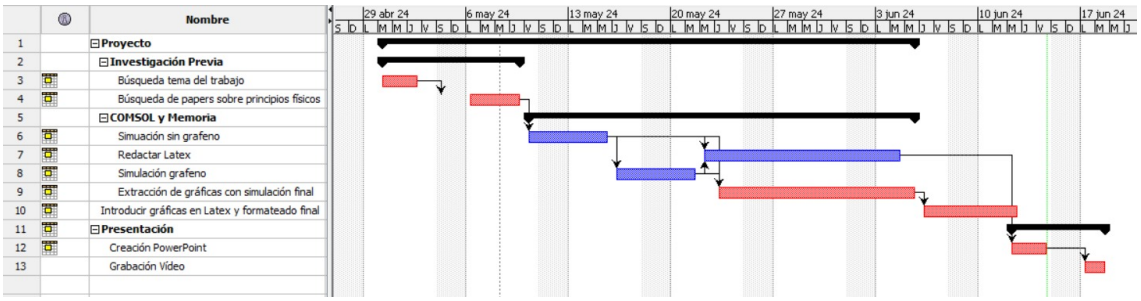

Figura 1: Gantt chart showing the tasks performed for the project, their durations, and dependencies.

In order to ensure a smooth workflow, all tasks were carefully planned and organized. Responsibilities included simulation work using COMSOL Multiphysics software, comprehensive documentation, project planning, Python-based graph generation, and preparation of the final presentation.
Initially, the project topic was determined after a thorough review of relevant literature to understand the underlying physics of the intended model. An initial simulation of a waveguide without graphene was then created to verify that the chosen methodology produced coherent results in line with existing studies.
Following this phase, the model was modified to analyze the impact of graphene. With simulation results obtained via COMSOL, documentation was developed that encompassed both the theoretical foundations and the data acquired and visualized using Python libraries and the simulation software.
After gathering all the necessary study data, the documentation was finalized with both theoretical and simulated components. Finally, the conclusions were presented in a recorded presentation.

2.2. Sustainable Development Goals

In a global context, the sustainable development goals addressed by this project are:

- **SDG 7: Affordable and clean energy.** Graphene-based waveguides can enhance the efficiency of communication and energy systems, reducing energy consumption and carbon emissions.
- **SDG 9: Industry, innovation, and infrastructure.** By fostering technological innovation and improving communication infrastructures, graphene drives the development of more advanced and sustainable industries.
- **SDG 11: Sustainable cities and communities.** The feasible applications of graphene and optical fibers enable ecological and efficient communication across cities and habitable areas.
- **SDG 12: Responsible consumption and production.** The production of graphene-based devices can be more sustainable and efficient, reducing the use of less efficient and more polluting materials.

- **SDG 13: Climate action.** By improving energy efficiency and reducing emissions, graphene applications directly contribute to combating climate change.

The impact of the project on each of the aforementioned SDGs has been evaluated, and the level achieved for each is shown in Figure 2.

Objetivos de Desarrollo Sostenibles	Alto	Medio	Bajo	No Procede
ODS 1. Fin de la pobreza				X
ODS 2. Hambre cero				X
ODS 3. Salud y bienestar				X
ODS 4. Educación de calidad				X
ODS 5. Igualdad de género				X
ODS 6. Agua limpia y saneamiento				X
ODS 7. Energía asequible y no contaminante	X			
ODS 8. Trabajo decente y crecimiento económico				X
ODS 9. Industria, innovación e infraestructuras	X			
ODS 10. Reducción de las desigualdades				X
ODS 11. Ciudades y comunidades sostenibles			X	
ODS 12. Producción y consumo responsables		X		
ODS 13. Acción por el clima		X		
ODS 14. Vida Submarina				X
ODS 15. Vida de ecosistemas terrestres				X
ODS 16. Paz, justicia e instituciones sólidas				X
ODS 17. Alianzas para lograr objetivos				X

Figura 2: Level achieved in each of the Sustainable Development Goals (SDGs).

2.3. Prior Knowledge

A waveguide is a structure through which electromagnetic or acoustic waves are transmitted. For electromagnetic waves, the structure, dimensions, and materials used vary greatly depending on the employed wavelength. Unlike metallic, hollow, rectangular waveguides used to conduct waves with wavelengths on the order of $10^1 \sim 10^{-6}$ m, in the optical domain the employed structure is an optical fiber. In an optical fiber, a core with a refractive index n_2 embedded in a cladding material with a refractive index $n_1 < n_2$ allows the wave to travel long distances with minimal losses thanks to the phenomenon of total internal reflection.
During the propagation of the wave through the waveguide, the concept of propagation modes is vital, that is, the different ways in which the electromagnetic field can arrange itself within the waveguide during propagation. These modes are determined by the application of Maxwell's equations along with the boundary conditions imposed by the waveguide and can be classified as:

- **TE (Transverse Electric) Mode:** The electric field component in the propagation direction is zero.
- **TM (Transverse Magnetic) Mode:** The magnetic field component in the propagation direction is zero.

A diagram of the first four propagated modes can be seen in Figure 3.

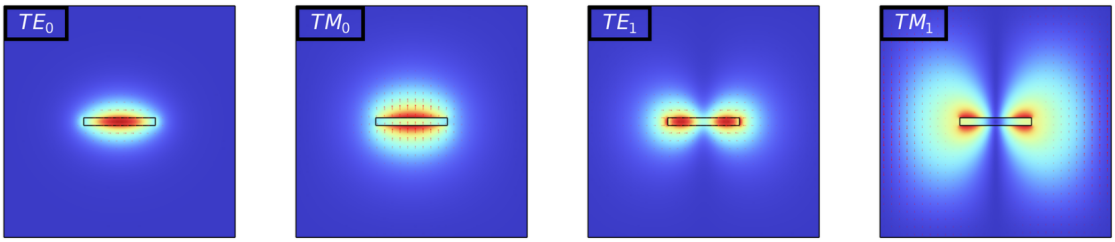

Figura 3: First four modes propagated by a planar optical waveguide, including transverse electric (TE_0, TE_1) and transverse magnetic (TM_0, TM_1) modes. A core with dimensions 200×1860 nm and a cladding with dimensions 6×6 μm were used.

2.4. Theoretical Description and Graphene Specificities

Graphene has generated exceptional interest as an optoelectronic material due to its high charge carrier mobility (greater than $200,000$ cm^2 V^{-1} s^{-1} [10]) and its wide absorption range [4]. Its two-dimensional structure consists of carbon atoms arranged in a hexagonal lattice. This arrangement causes the electrical and optical properties of graphene to vary depending on the direction in which waves or currents propagate through it, making the material anisotropic. This anisotropy arises mainly from variations in electron interactions along different directions in the graphene plane, with significant implications for optics and electronics.
In this study, the wide absorption range of graphene will be exploited to strongly attenuate electromagnetic waves by placing a graphene film at the field maximum.

2.4.1. Conductivity Model

To incorporate the absorption of graphene into this study, its impedance as a material will be defined, which is obtained from its conductivity simply as its inverse [11]:

$$Z_{gr} = \frac{1}{\sigma_g} \tag{1}$$

This approach establishes its absorption property from the perspective of conductivity, with absorption occurring when the mode impedance matches the graphene impedance, acting as a circuit where graphene functions as a resistor that cuts the current flow without transmission or reflection.
The optical conductivity of graphene, σ_g, depends on the temperature, T, the angular frequency, ω, the Fermi level, μ, and the relaxation rate, Γ. This conductivity can be described as the sum of two types of conductivity classified based on the carrier transitions as interband and intraband [1]:

$$\sigma_g(\omega, \mu, \Gamma, T) = \sigma_{inter} + \sigma_{intra} \tag{2}$$

Where the interband conductivity, due to transitions of electrons between the conduction band and the valence band, can be described as:

$$\sigma_{inter} = \frac{-ie^2}{4\pi\hbar} \ln \frac{2|\mu| - \hbar\omega_0 + 2i\Gamma}{2|\mu| + \hbar\omega_0 - 2i\Gamma} \tag{3}$$

And the intraband conductivity, due to transitions of electrons within the same band, can be described as:

$$\sigma_{intra} = \frac{-ie^2 k_B T}{\pi(\hbar^2\omega_0^2 - 2i\Gamma^2)} \times \left(\frac{\mu}{k_B T} + 2\ln(1 + e^{-\mu/k_B T}) \right) \tag{4}$$

However, it can be observed that the formula for intraband conductivity is dimensionally incorrect, as the quotient on the left has units of farads (F), while the term on the right is dimensionless. To achieve units of siemens (S), it was necessary to multiply by the inverse of a relaxation time τ, used in other studies on graphene conductivity [12], and it has been verified that it does not affect normalized values. The total conductivity for the employed equations, both in its imaginary and real components, has been plotted as shown in Figure 4.

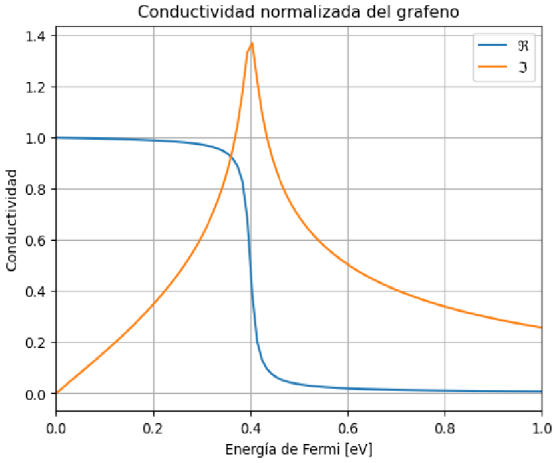

Figura 4: Normalized conductivity of graphene for the considered equations, both in its real ($\Re$) and imaginary ($\Im$) components.

2.5. Implementation with COMSOL Multiphysics

2.5.1. Operation of the software used

COMSOL Multiphysics is a commercial software that uses the finite element method to simulate models applicable to various physical and engineering applications. The resolution of a problem with COMSOL always follows the same structure, which can be summarized in the following steps:

- **Selection of spatial dimension.** The software allows simulations for two-dimensional, three-dimensional, or axisymmetric systems, among others. It is necessary to select the most appropriate option for the study to be conducted, always seeking to simplify the problem as much as possible to save computational resources.
- **Definition of parameters and variables.** Before defining the geometry and introducing values, it is necessary to define the parameters and constants to be used in the rest of the study. Referring all subsequent steps to these values is crucial, as it allows quick modifications to parametrically defined parts by simply adjusting the corresponding variables. Additionally, the software enables the definition of variables, integrals, and functions, which can later be used to describe the behavior of certain parts of the model.
- **Definition of geometry.** The software allows importing geometries or defining them directly within the program using basic two-dimensional or three-dimensional shapes, depending on the type of study. More complex geometries can be created using Boolean operations.

- **Material assignment.** Each domain of the geometry must be identified as a specific material. The program provides a library of predefined materials but also allows the creation of custom materials from relevant physical parameters for the employed physics module.
- **Introduction of physics and boundary conditions.** Depending on the physical application of the model, the appropriate physics module and its equations must be imported. For complex cases, it is possible to link modules and implement multiphysics. Next, all initial conditions, physical fields, and approximations in the geometry must be assigned. The software includes conditions applicable to edges or surfaces, which in some cases require initial values such as power or pressure (for incident pressure or electromagnetic waves, for example).
- **Mesh generation.** Before computing the model, it is necessary to discretize the volume (in the 3D case) or surface (2D case) to apply the finite element method. The mesh can be created automatically or manually, allowing customization of element shape or size, among other options. It is worth noting that special conditions must be met for the mesh when certain boundary conditions are introduced. For instance, it must be identical on faces that exhibit periodic symmetry, which can be achieved using special software options that copy mesh parts between faces.
- **Study creation.** Once the physics, geometry, materials, and mesh are defined, the software must be instructed on what to calculate. This is done by defining studies, which vary depending on the applied physics model. Default studies include eigenvalue calculations, resonance mode analysis, or stationary calculations. These studies can be customized and enhanced using tools like parameter sweeps or optimization.
- **Result analysis.** After computing the studies, the software allows the definition of lines, two-dimensional cuts, or three-dimensional regions to visualize certain parameters of interest in the physical model. It also enables plotting parameters against each other in simple graphs.

For both the preliminary case and the case of interest, the *2D component* option available in COMSOL Multiphysics was used. This decision was primarily due to the limited computational resources and because the waveguide is essentially symmetric along its axis, so a cross-sectional representation accurately reproduces its real behavior. Both models utilized the *Electromagnetic Waves*, *Frequency Domain* (*ewfd*) module and the *Mode Analysis* study.

2.5.2. Preliminary Case: Waveguide without Graphene

Before simulating the case of interest, a waveguide with identical materials but without the graphene layer was simulated. This waveguide consists of a SiN core surrounded by a silicon dioxide (SiO_2) cladding.
The geometry was parametrically designed, centering the waveguide core on the coordinate axis and establishing an arbitrary cladding width, considering the core as embedded in an infinite medium. To account for this assumption, the *Scattering Boundary Condition* was added to the outer edges of the cladding in the physics settings.
The materials were defined from scratch using the *blank material* option and defining both SiN and SiO_2 based on their refractive indices: $n_{SiN} = 2{,}02$ and $n_{SiO_2} = 1{,}4464$.
Due to the simplicity of the geometry, a simple triangular mesh was used throughout the model, ensuring the core was evenly and uniformly covered.
Two studies were defined. First, a *parametric sweep* was conducted along with a *mode analysis* to determine the effective refractive index of the first four propagated modes as a function of the

core width. This aimed to identify the range of core dimensions for which the modes of interest (TE_0 and TE_1) propagate.
In the second study, the core width parameter was fixed at $W = 1{,}86\ \mu m$, and the *mode analysis* was repeated to calculate and visualize the electric field magnitude within the waveguide and at the upper edge of the core (where the graphene-core interface would exist in the case with graphene) for objective comparison with the second case.

2.5.3. Case of Interest: Waveguide with Graphene

The waveguide with graphene study was based on the same simulation as the previous case, using a SiN core and SiO_2 cladding with an optimized core width of $W = 1{,}86\,\mu m$ calculated in the prior study.
For simplicity in terms of computation, the case of graphene as a filter for the TE_0 mode was simulated. A new rectangle with a height of $0{,}1\,nm$ was added directly above and centered on the core, as this point corresponds to the maximum electric field for that mode. The graphene height was chosen arbitrarily, as variations in thickness (up to $0{,}3\,nm$) have negligible effects on mode absorption [2].
In this case, graphene is neither implemented as a blank material nor as a predefined material from the COMSOL library. Instead, its absorption properties are established by defining its impedance as a material, as explained in Section 2.4.1.
This approach avoids declaring graphene as an anisotropic material since its absorption property is defined from the perspective of conductivity. This conductivity is defined in COMSOL under the *Definitions* section, following Equation (1) previously developed.
Initially, intraband conductivity was neglected because it becomes significant at THz frequencies, and it was assumed that the study would involve higher frequencies. However, for the studied wavelength, it was found necessary to consider its contribution. After defining the required parameters, these formulas were implemented as variables, and impedance was also defined. To implement these graphene properties, the *Surface Current Density* condition was defined in the physics module. By selecting graphene as the domain, the surface current density in the X-axis was set as $ewfd.E_x/Z_{gr}$, establishing the behavior of the layer as graphene.
Lastly, due to the thinness of the graphene film, the mesh had to be customized to avoid errors, ensuring it aligned with the physics of the model, specifically with the employed wavelength.
Once graphene was defined, several studies were conducted. First, a *parametric sweep* was performed over values of the Fermi energy μ (an experimentally adjustable parameter through voltage), varying the material's absorption capacity. This also aimed to verify the feasibility of implementing a filtering system for both modes, selectable based on the voltage applied to the graphene sheets [12]. Absorption capacity can be measured using either the absorption coefficient or the absorbed power. The former can be calculated as [2]:

$$\alpha = 40\pi(\log_{10} e)\Im(n_{neff})/\lambda \tag{5}$$

And the latter as [13]:

$$P = \int_V \sigma |\mathbf{E}|^2 dv \tag{6}$$

Where V represents the total domain of the geometry. The integral had to be implemented beforehand in COMSOL's *Definitions* section, and power was calculated as a variable in the same section.
Additionally, a study was conducted on the absorption of TE_0 modes for various widths of the graphene film, specifically from $300\,nm$ to $500\,nm$, and repeated for $\mu = 0{,}2\ eV$, $\mu = 0{,}4\ eV$,

and $\mu = 0{,}8\ eV$. The range of widths was selected for a manageable number of values and a relatively small interval, as increasing the film size makes computations less efficient. However, this range is sufficient to observe absorption effects. A *parametric sweep* was performed for the parameter W_g, the width of the graphene film.

This study aimed to examine the dependence of mode absorption on film width by observing and interpreting the magnitude of the electric field within the core and at the interface between the graphene and the core. The goal was to study the absorption coefficient of graphene, expecting to achieve absorption for the TE_0 mode and no absorption for the TE_1 mode.

To observe the results of this last study, two *Cut Line 2D* data lines were defined: one along the waveguide core and another at the interface between the core and graphene.

3. Results

3.0.1. Preliminary Case: Waveguide without Graphene

First, the range within which the waveguide core width must fall for the modes of interest (TE_0 and TE_1) to propagate was successfully determined. Subsequently, an appropriate value within this range was selected for further studies.

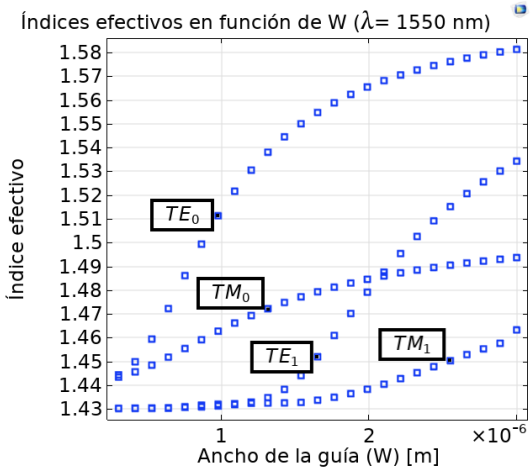

Figura 5: Real part of the effective indices of the first four propagated modes as a function of W, the waveguide core width. Refractive indices were calculated for $\lambda = 1550$ nm and a range of $W = 0{,}3\ \mu m$ to $W = 3\ \mu m$.

As shown in Figure 5, obtained with a *parametric sweep* between 0.3 and 3 μm, the range is between 1.5 and 2 μm, since beyond two microns, the TM_1 mode begins to propagate, and for a width smaller than this range, the TE_1 mode does not propagate. We observe that the dimensions considered in similar works correspond to the calculated range [2]. With the value used by other researchers being $W = 1{,}86\ \mu m$, this value has been considered appropriate and will be used henceforth.
Secondly, the electric field distribution along the X-axis was obtained for the two modes of interest (TE_0 and TE_1), as shown in Figure 6. In the left graph, extracted using a *1D plot group*, the electric field norm shows a Gaussian shape for the TE_0 mode, reaching a maximum of 75 V/m at the center of the waveguide. For the TE_1 mode, there are two equal and symmetric maxima around 0, reaching approximately 35 V/m. In the two graphs on the right, obtained with a *2D plot group*, the cross-section of both modes corresponds to the findings of the previous graph.
Finally, as shown in Figure 7, at the upper edge of the core, the field has a similar distribution to the center. However, the magnitude of the values is much lower, presumably because the mode is confined within the core and is not being absorbed at the interface.

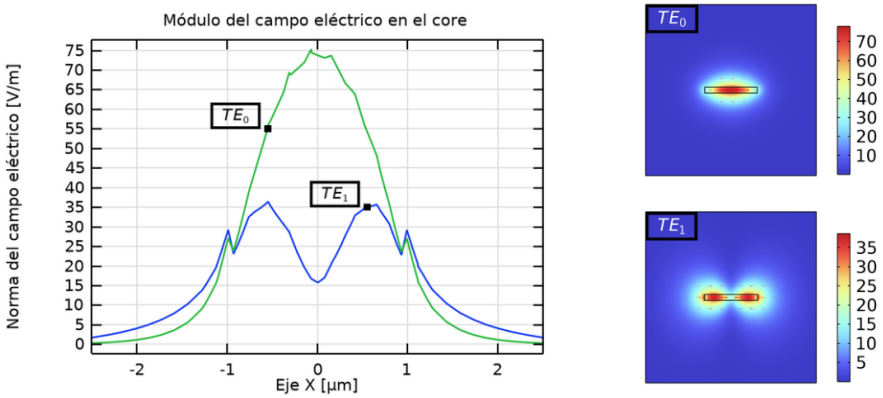

Figura 6: Electric field magnitude along the X-axis of the waveguide for the TE_0 and TE_1 modes, along with their cross-sectional field representations.

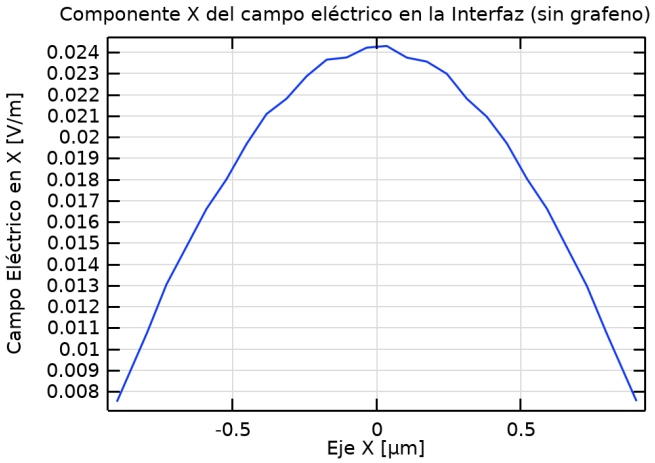

Figura 7: X-component of the electric field along the upper edge of the waveguide core for the TE_0 mode.

3.0.2. Case of Interest: Waveguide with Graphene

First, the results for the absorption coefficients and absorbed power of the modes were analyzed for an initial graphene film width of 300 *nm* as a function of the Fermi energy. This width was chosen as it was used in other related studies [2].
As seen in Figure 8, three distinct regions can be identified. In the first region, for $\mu < 0{,}4\ eV$, a high degree of absorption is observed. In the second region, at $\mu \approx 0{,}4\ eV$, there is a transition to a low-loss region. Finally, in the third region, for $\mu > 0{,}4\ eV$, minimal absorption is observed [12].
For the TE_0 mode, the distinction between regions is very pronounced compared to the TE_1 mode, which is an order of magnitude lower and appears to remain constant. This is logical since the graphene film is positioned specifically to absorb the TE_0 mode and not the TE_1 mode.
Furthermore, the correctness of the behavior can be confirmed by observing the absorbed power plots, which exhibit the same behavior as the absorption coefficient. This power is calculated using Equation (6).
Since the behavior is the same, subsequent results will focus solely on the absorption coefficient, as it accurately represents graphene's behavior.
Once it was observed that three different absorption regions exist as a function of Fermi energy,

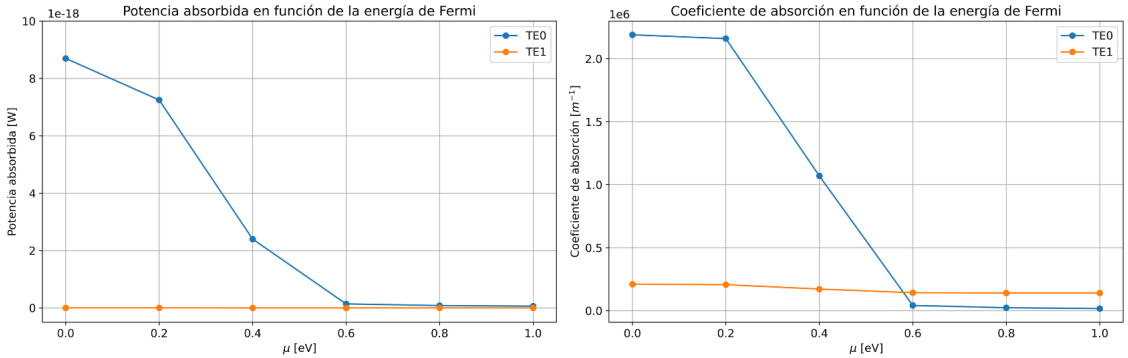

Figura 8: Absorbed power (left) and absorption coefficient (right) as a function of Fermi energy μ, for a graphene film width $W_g = 300\ nm$.

the effect of the graphene film width was studied in each region, varying between 300 nm and 500 nm. The study was conducted for $\mu = 0{,}2\ eV$, $\mu = 0{,}4\ eV$, and $\mu = 0{,}8\ eV$.
For the graphene absorption study, the *Cut Line 2D* within the core was initially used to study how the electric field norm varies as a function of the guide width for both modes. The study was conducted for $\mu = 0{,}2\ eV$, $\mu = 0{,}4\ eV$, and $\mu = 0{,}8\ eV$. Figure 9 shows the case for $\mu = 0{,}4\ eV$, which provided results closest to theoretical expectations.

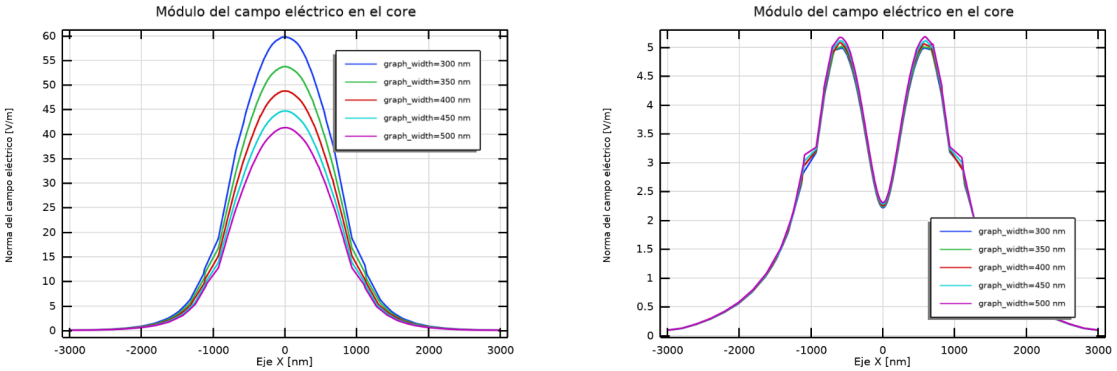

Figura 9: Electric field magnitude for the TE_0 mode (left) and TE_1 mode (right), for a Fermi level $\mu = 0{,}4\ eV$ as a function of graphene width.

As expected, as the film width increases, the TE_0 mode is absorbed more effectively. On the other hand, the TE_1 mode, despite showing reduced absorption compared to the waveguide without graphene (a phenomenon explained by the confinement of this mode within the core), remains almost constant for different guide widths. This is logical since the film's location is not optimal for absorbing the second mode.
However, it was determined that the electric field norm is not the optimal parameter for visualizing the film's effects, as COMSOL may account for other field components or involuntary factors. An example of such erroneous behavior is that the graphs for $\mu = 0{,}2\ eV$ and $\mu = 0{,}8\ eV$ are nearly identical, which does not align with the absorption coefficient observed for different Fermi energies (for $\mu = 0{,}2\ eV$, greater absorption should be evident, as shown in Figure 8).
To investigate the previously observed incoherent behavior, the *Cut Line 2D* at the graphene-core interface was used as the dataset, and the X-component of the electric field (the characteristic axis of TE modes) was plotted.
As shown in Figure 10, peaks are observed at the edges of the graphene film, caused by the

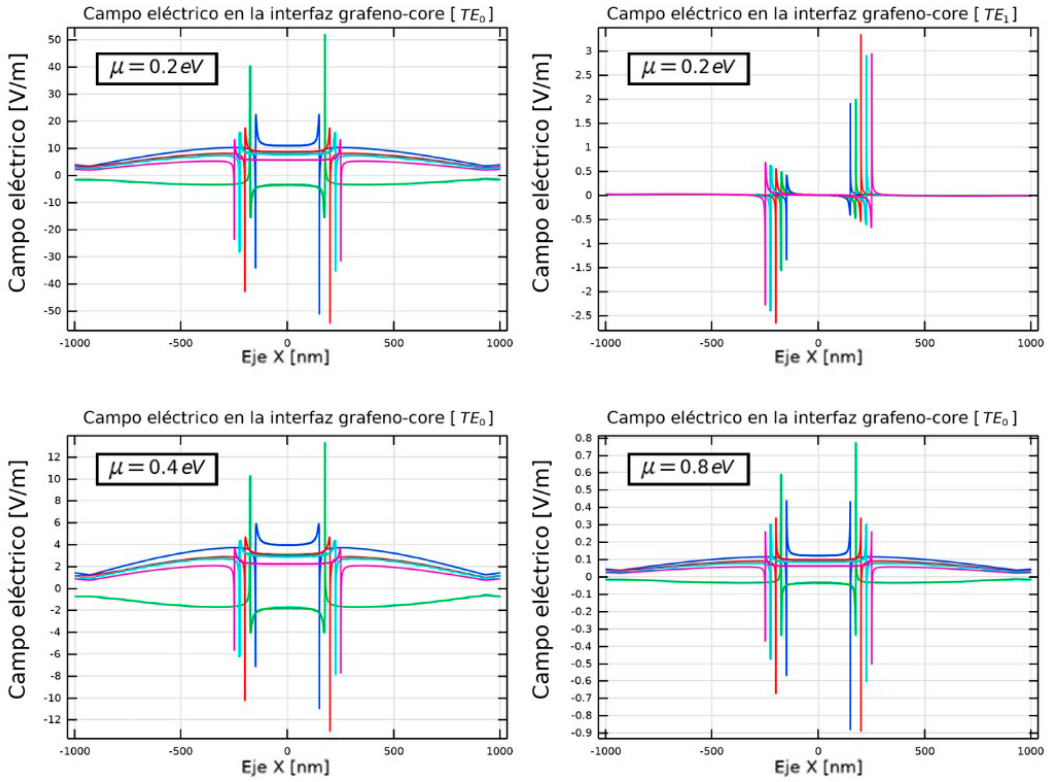

Figura 10: X-component of the electric field at the graphene-core interface as a function of the film width, for four different cases: TE_0 mode with $\mu = 0{,}2\ eV$ (top left), TE_1 mode with $\mu = 0{,}2\ eV$ (top right), and TE_0 modes with $\mu = 0{,}4\ eV$ and $\mu = 0{,}8\ eV$ (bottom left and right, respectively). The colors pink, turquoise, red, green, and blue denote film widths of 500, 450, 400, 350, and 300 *nm*, respectively.

abrupt change of medium. These peaks become increasingly separated, marking the start and end of the film. Unlike the results obtained by plotting the electric field magnitude, these graphs demonstrate a coherent relationship between the electric field and the Fermi energy, consistent with the initial study of the case (see Figure 8). For $\mu = 0{,}2\ eV$, the electric field is significantly higher than for $\mu = 0{,}8\ eV$. This is logical since the electric field at the interface corresponds to the field being absorbed by graphene. At $\mu = 0{,}2\ eV$, the high electric field indicates significant absorption, whereas at $\mu = 0{,}8\ eV$, the opposite occurs, with most of the field propagating within the core. At $\mu = 0{,}4\ eV$, an intermediate value is observed.

These results are opposite to those obtained when visualizing the electric field at the core edge for the case without graphene, where minimal interaction was observed in this region. By implementing the graphene film on the core, the field is absorbed, substantially increasing the magnitude of the X-component of the electric field.

Conversely, for the TE_1 mode, the graph at the interface shows minimal variation, remaining at zero regardless of the graphene film width or the Fermi energy. This is consistent with the film geometry being designed to absorb the TE_0 mode. Only the $\mu = 0{,}2\ eV$ case was plotted due to its similarity to results obtained for other Fermi energy values.

To support these discussions about absorption as a function of width, the absorption coefficient for both modes was also plotted as a function of the graphene film width and for different Fermi energy values (see Figure 11).

As shown, the results align with previous discussions. On one hand, the absorption coefficient

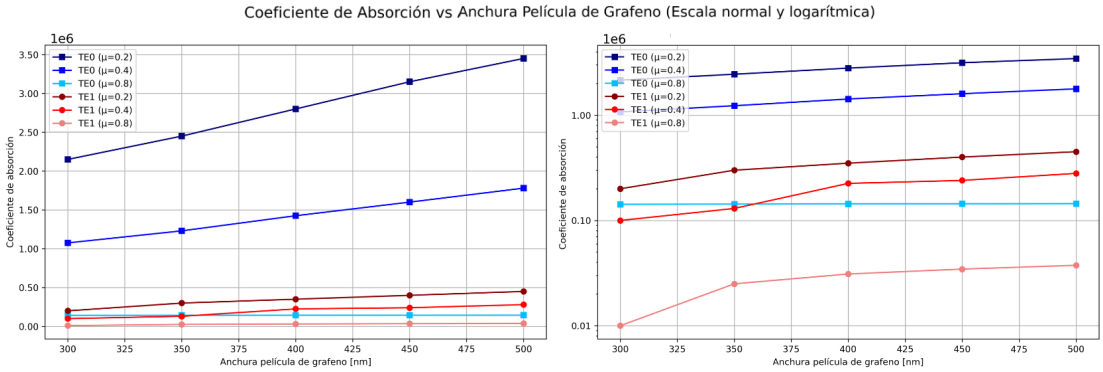

Figura 11: Absorption coefficient of TE_0 (blue) and TE_1 (red) modes for different graphene film widths and Fermi levels (μ). Both natural (right) and logarithmic (left) scales are used to better visualize lower values.

increases with the film width, consistent with the decrease in the electric field magnitude for the TE_0 mode, while the TE_1 mode remains nearly constant, as reflected in the absorption coefficients, which show little variation with width. On the other hand, for each Fermi energy, the absorption coefficient decreases as the Fermi level increases. An interesting behavior is observed for $\mu = 0{,}8\ eV$, where the coefficient remains nearly constant despite the increasing film width. This is logical, as absorption in this region is minimal.

4. Conclusions

After conducting the studies and analyzing the results, it is concluded that graphene films can be effectively used to absorb propagating modes in a waveguide. Specifically, it has been verified that the TE_0 mode can be attenuated using a film positioned at X = 0, and this attenuation is proportional to the film width. Furthermore, it has been demonstrated that the absorption level can be adjusted to allow or block the mode by modifying the Fermi energy through a voltage applied to the film.
It should be noted that some discrepancies or errors may exist in this project, as the study of graphene is highly complex and detailed. Some data might have been overlooked, or certain graphs may not fully align with reality. For example, the graph in Figure 9 has been interpreted as unrealistic due to inconsistencies and is assumed to result from a COMSOL calculation error. This assumption is supported by the graphene-core interface graphs, but further verification is needed to identify the precise cause. One possibility is an error in the implementation of graphene conductivity, as the plotted results (see Figure 4) do not exactly match findings from other studies in the field [1], particularly regarding the decline of the imaginary part of conductivity, as shown in Figure 12.

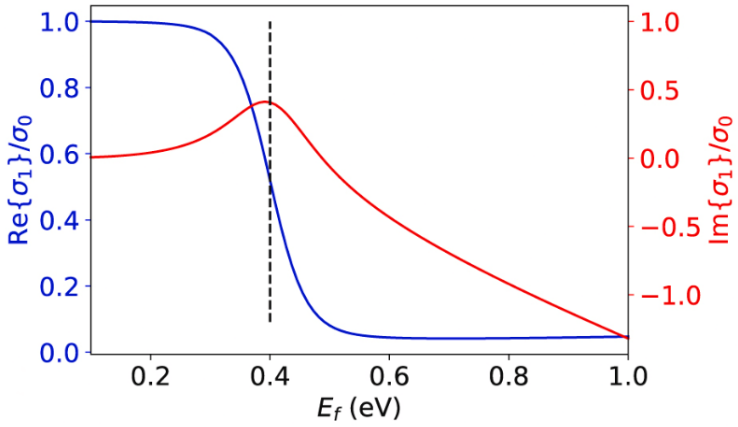

Figura 12: Normalized conductivity of graphene for the considered equations, both real ($\Re$) and imaginary ($\Im$), from [1].

For a more comprehensive project, studies on graphene as a filter for the TE_1 mode should be conducted, placing graphene films on both sides of the waveguide core. This new configuration would involve analyzing absorption behavior for this mode, including its dependence on Fermi energy and film width, as well as the effect of film spacing on absorption. This would further confirm the validity and utility of this study.
In any case, this study confirms that graphene can indeed be used as an optical mode filter, enabling the complete implementation of a mode-division multiplexor for TE_0 and TE_1 modes. This could be achieved using the design shown in Figure 13. Filters would be activated based on the voltage applied to the graphene films, altering their Fermi energy and placing the material in either a high or low absorption state, a technique known as Mode Division Multiplexing (MDM).

4.1. Future Potential and Research Impact

As determined in the conclusions, the application of graphene in waveguides opens the door to Mode Division Multiplexing (MDM), a technology revolutionizing optical communications.

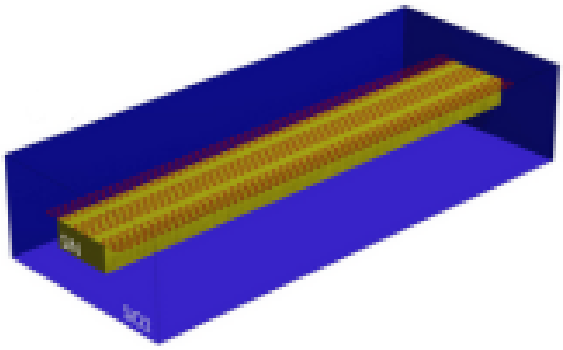

Figura 13: Waveguide design with graphene as an absorber for TE_0 and TE_1 modes, from [2].

The technique developed in this study has significant potential in communications, as it can greatly enhance data transmission capacity through waveguides. Since it does not require multiple precise-wavelength laser sources, it becomes a cost-effective method to scale optical network capacity.
Additionally, this work paves the way for promising improvements in photonic sensing devices by integrating graphene into their structures. Graphene's unique properties, such as high charge mobility and wide absorption range, can further enhance their efficiency.
Specifically, waveguides with graphene can be integrated into optical interferometry devices, surface plasmon resonance (SPR) sensors, and fiber Bragg grating (FBG) sensors [14]. Due to graphene's high electron mobility and large surface area, efficient absorption of gas molecules and biomolecules is achieved, enabling precise signal modulation and highly sensitive detection of environmental and biological parameters. These properties make graphene-based sensors highly suitable for biomedical applications, allowing non-invasive biomarker detection in bodily fluids, which is crucial for continuous patient monitoring [15].
Moreover, graphene-coated fiber optic sensors can be used in harsh environments and extreme temperatures, offering high sensitivity and rapid response times.
In conclusion, these applications demonstrate how graphene-enhanced waveguides can revolutionize current sensing and communication technologies.

Referencias

[1] Tamura, M., Morison, H., Shastri, B. J. "Inducing optical self-pulsation by electrically tuning graphene on a silicon microring." *Nanophotonics* **11.17** 4017–4025 (2022).

[2] Martín-Romero, F., Gómez, V. J. "Design and Optimization of a Graphene-On-Silicon Nitride Integrated Waveguide Dual-Mode Electro-Absorption Modulator." (2024) URL https://api.semanticscholar.org/CorpusID:267301427.

[3] Liu, M., *et al.* "A graphene-based broadband optical modulator." *Nature* **474.7349** 64–67 (2011) doi:10.1038/nature10067 URL https://doi.org/10.1038/nature10067.

[4] Bonaccorso, F., Sun, Z., Hasan, T., Ferrari, A. C. "Graphene photonics and optoelectronics." *Nature Photonics* **4.9** 611–622 (2010) doi:10.1038/nphoton.2010.186 URL https://doi.org/10.1038/nphoton.2010.186.

[5] Kim, K., Choi, J.-Y., Kim, T., Cho, S.-H., Chung, H.-J. "A role for graphene in silicon-based semiconductor devices." *Nature* **479.7373** 338–344 (2011) doi:10.1038/nature10680 URL https://doi.org/10.1038/nature10680.

[6] Phare, C. T., Daniel Lee, Y.-H., Cardenas, J., Lipson, M. "Graphene electro-optic modulator with 30GHz bandwidth." *Nature Photonics* **9.8** 511–514 (2015) doi:10.1038/nphoton.2015.122 URL https://doi.org/10.1038/nphoton.2015.122.

[7] Gan, X., *et al.* "Chip-integrated ultrafast graphene photodetector with high responsivity." *Nature Photonics* **7.11** 883–887 (2013) doi:10.1038/nphoton.2013.253 URL https://doi.org/10.1038/nphoton.2013.253.

[8] Xing, Z., *et al.* "Waveguide-integrated graphene spatial mode filters for on-chip mode-division multiplexing." *Opt. Express* **27.14** 19188–19195 (2019) doi:10.1364/OE.27.019188 URL https://opg.optica.org/oe/abstract.cfm?URI=oe-27-14-19188.

[9] Wang, J., Zhang, X., Chen, Y., Geng, Y., Du, Y., Li, X. "Design of a graphene-based silicon nitride multimode waveguide-integrated electro-optic modulator." *Optics Communications* **481** 126531 (2021) doi:https://doi.org/10.1016/j.optcom.2020.126531 URL https://www.sciencedirect.com/science/article/pii/S0030401820309494.

[10] Xia, F., Mueller, T., Lin, Y.-m., Valdes-Garcia, A., Avouris, P. "Ultrafast graphene photodetector." *Nature Nanotechnology* **4.12** 839–843 (2009) doi:10.1038/nnano.2009.292 URL https://doi.org/10.1038/nnano.2009.292.

[11] Wang, X., Tretyakov, S. A. "Toward Ultimate Control of Terahertz Wave Absorption in Graphene." *IEEE Transactions on Antennas and Propagation* **67.4** 2452–2461 (2019) doi:10.1109/TAP.2018.2889144.

[12] Faneca, J., Hogan, B. T., Diez, I. R., Gardes, F. Y., Baldycheva, A. "Tuning silicon-rich nitride microring resonances with graphene capacitors for high-performance computing applications." *Opt Express* **27.24** 35129–35140 (2019).

[13] Ellingson, S. W. [Accessed 07-06-2024] "6.6: Power Dissipation in Conducting Media — eng.libretexts.org." https://eng.libretexts.org/Bookshelves/Electrical_Engineering/Electro-Optics/Book:_Electromagnetics_I_(Ellingson)/06:_Steady_Current_and_Conductivity/6.06:_Power_Dissipation_in_Conducting_Media.

[14] Hernaez, M., Zamarreño, C. R., Melendi-Espina, S., Bird, L. R., Mayes, A. G., Arregui, F. J. "Optical Fibre Sensors Using Graphene-Based Materials: A Review." *Sensors (Basel)* **17.1**.

[15] Kim, H., Ahn, J.-H. "Graphene for flexible and wearable device applications." *Carbon* **120** 244–257 (2017) doi:https://doi.org/10.1016/j.carbon.2017.05.041 URL `https://www.sciencedirect.com/science/article/pii/S0008622317304876`.